SCIENCE CHINA
Information Sciences

• RESEARCH PAPER •
Special Focus on Geosynchronous Synthetic Aperture Radar

June 2017, Vol. 60 060303:1–060303:15
doi: 10.1007/s11432-016-9083-4

Optimal 3D deformation measuring in inclined geosynchronous orbit SAR differential interferometry

Cheng HU[1,2], Yuanhao LI[1*], Xichao DONG[1], Rui WANG[1] & Chang CUI[1]

[1]*School of Information and Electronics, Beijing Institute of Technology, Beijing* 100081*, China;*
[2]*Key Laboratory of Electronic and Information Technology in Satellite Navigation* (*Beijing Institute of Technology*)*, Ministry of Education, Beijing* 100081*, China*

Received December 16, 2016; accepted April 21, 2017; published online May 16, 2017

Abstract Three dimensional (3D) deformation can be obtained by using differential interferometric synthetic aperture radar (D-InSAR) technique with the cross-heading tracks data of low earth orbit (LEO) SAR. However, this method has drawbacks of the low temporal sampling rate and the limited area and accuracy for 3D deformation retrieval. To address the aforementioned problems, by virtue of a geosynchronous (GEO) SAR platform, this paper firstly demonstrates the expressions of 3D deformation and the corresponding errors in GEO SAR multi-angle processing. An optimal multi-angle data selection method based on minimizing position dilution of precision (PDOP) is proposed to obtain a good 3D deformation retrieval accuracy. Moreover, neural network is utilized for analyzing the accuracy of the retrieved 3D deformation under different orbit configurations and geo-locations. Finally, the proposed methods and the theoretical analysis are verified by simulation experiments. A 3D deformation retrieval accuracy of the order of centimeter-level or even millimeter-level can be obtained by using the selected optimal multi-angle data.

Keywords geosynchronous synthetic aperture radar (GEO SAR), three dimensional (3D) deformation measurement, multi-angle processing, differential SAR (D-InSAR), neural network

Citation Hu C, Li Y H, Dong X C, et al. Optimal 3D deformation measuring in inclined geosynchronous orbit SAR differential interferometry. Sci China Inf Sci, 2017, 60(6): 060303, doi: 10.1007/s11432-016-9083-4

1 Introduction

Synthetic aperture radar differential interferometry (D-InSAR) plays an important role in the large-coverage high-accuracy measurement of deformation caused by geological disasters (e.g. earthquake, land subsidence, and landslide) [1, 2]. However, conventional D-InSAR technique can only obtain the deformation information of the scene in the direction of line of sight (LOS), being insensitive to the other components of the deformation. In the natural environment, many geological activities (such as fault movements and volcano movements) give rise to deformations in the three dimensions (3D) [3–5]. Therefore, a LOS D-InSAR measurement technique is not enough to truly understand the deformation patterns of geological activities.

To deal with the limitation of the D-InSAR one dimensional (1D) measurement, the methods based on the low earth orbit (LEO) SAR multi-angle observations [5, 6] and the combined processing of global

* Corresponding author (email: lyh.900101@163.com)

positioning system (GPS) data and 1D LEO D-InSAR data [7] were proposed. However, their realizations and processing accuracies are limited by the LEO SAR satellite configuration and the density of GPS reference points. Moreover, LEO SAR 3D deformation retrieval will be limited by the long revisit time and the small coverage area of LEO SAR. Due to the aforementioned shortcomings, 3D deformation measurement based on LEO SAR system is difficult to be carried out in practical geological applications.

In order to overcome the drawbacks of traditional LEO SAR orbits in 3D deformation retrieval and obtain the ideal multi-angle data, a geosynchronous SAR (GEO SAR) system for 3D deformation retrieval is proposed. A GEO SAR runs in a geosynchronous orbit (about 36000 km above the Earth surface) and has been deeply studied for more than thirty years [8–13]. Lots of studies in GEO SAR imaging algorithms [14–19], impact of atmospheric disturbances on GEO SAR [20–22], and GEO SAR interferometry applications [23] have been carried out. Because of the high running orbit, GEO SAR has less than one day revisit time. Moreover, since GEO SAR can be continuously steered due to its phase array antenna capability of two dimensional (2D) beam scanning and flexible beamforming [24], a coverage area of the order of 1000 km and an illuminating time longer than several hours for the scene of interest (providing lots of view angles) can be obtained. 3D deformation retrieval by GEO SAR has been conceived firstly by national aeronautic and space administration (NASA) in its global earthquake satellite system (GESS) project [24]. The expected 3D displacement accuracy can reach to a few millimeters after 24–36 h due to lots of GEO SAR images achieved in abundant view angles. Moreover, based on the study of the ideal GEO circular trajectory SAR (CSAR) system, it has been proved that 3D deformation retrieval can be realized by using at least three sub-apertures measurements [25].

However, because GEO SAR system has the abundant data acquisition ability (long observation time towards the target), there are several key issues needed to be solved in GEO SAR 3D deformation retrieval by multi-angle processing. Firstly, to obtain the optimal 3D deformation retrieval accuracy, it is necessary to determine the optimal multi-angle data selection method for carrying out the 3D deformation retrieval. A reasonable criterion for the selection must to be designed. Secondly, because of the various designs of GEO SAR orbit and the large geographical area of the observed scene, to analyze the 3D deformation retrieval accuracy under different designed orbit configurations and observation regions should be done.

To address the aforementioned issues, in Section 2, the key technologies and limitations of GEO D-InSAR 1D deformation measurement are summarized. In Section 3, the 3D deformation retrieval method based on GEO SAR multi-angle processing is demonstrated, and expressions of 3D deformation and the corresponding errors are obtained. Moreover, based on the concept of position dilution of precision (PDOP) in the global navigation satellite system (GNSS), an optimal GEO SAR multi-angle data selection method by virtue of the criterion of minimizing PDOP is proposed, which effectively improves 3D deformation retrieval accuracy. In addition, the method of analyzing 3D deformation retrieval accuracy under the different orbit configurations and regions based on neural network is proposed. Finally, the proposed theoretical methods and the corresponding analysis are verified by the simulation experiments in Section 4. The results show that under the condition of the selected optimal multi-angle data, millimeter-level deformation retrieval accuracy can be obtained in the vertical direction, and deformation retrieval accuracies in the east-west and north-south directions are centimeter-level. Moreover, the 3D deformation retrieval accuracies under the different orbit configurations (large "figure 8", small "figure 8" and "figure O" GEO SAR orbits) and different geo-locations (China region) are analyzed. The large "figure 8" orbit has the best holistic 3D deformation retrieval accuracy (reaches to centimeter-lever). Finally, the paper is concluded in Section 5.

2 GEO D-InSAR: 1D deformation measuring and the limitation

2.1 Research progress in GEO D-InSAR

Due to the advantages of the short revisit time and the large coverage of GEO SAR systems, there have

been a lot of conceptions for deformation measurements by using GEO D-InSAR over the last decade. Hobbs et al. [10, 26] proposed and analyzed the performance of the high inclination GEO SAR system (monostatic and bistatic SAR) for interferometry processing. The analysis suggests that the spatial decorrelation is negligible for a GEO SAR system, although the perpendicular baseline even reaches to more than one kilometer length. Based on two GEO SAR orbits with high inclination (figure '8' orbit and figure 'blob'), Hu et al. [27] analyzed the variation of the repeat-pass perpendicular baseline generated by the orbital perturbation in the GEO SAR case, which could show that the GEO InSAR processing is feasible in the presence of the impact of the perturbation. Monti-Guarnieri et al. [28] proposed the geosynchronous earth monitoring by interferometry and imaging (GEMINI) system, which uses GEO SAR constellation system for interferometric measurements. The interferometric baseline is formed by a primary passive illuminator (placed on a communications satellite) and a pair (more pairs) of very light passive SAR receivers located close to the small satellite. Subsequently, Monti-Guarnieri et al. also proposed a number of GEO D-InSAR systems based on a GEO SAR multiple-input multiple-output (MIMO) system. Broquetas et al. [29] analyzed satellite orbital drift effects on the interferograms and the station-keeping requirements of different orbits with various orbital elements (eccentricity) and geographical positions (satellite nominal longitude).

With respect to the key technologies in GEO D-InSAR, the optimal minimal rotational-induced decorrelation (OMRD) InSAR data acquisition method [23] and the study on the impacts of the temporal-spatial variant background ionosphere on repeat-track GEO D-InSAR system [30] had been studied. The optimal InSAR data acquisition method is an important aspect of GEO D-InSAR data processing. Because of working at the geosynchronous orbit, GEO SAR is impacted by the complex orbital perturbation forces [27]. Resultantly, the repeated tracks of GEO InSAR are un-parallel. The un-parallel tracks will cause the mismatches of the azimuthal spatial spectra of the InSAR pair when the zero-Doppler centroids (ZDC) data acquisition in LEO InSAR is utilized [27]. Under this case, the obvious rotation-induced decorrelation will be generated in the InSAR pair. Because of the rotation-induced decorrelation, the correlation coefficient of the interferogram will be less than 0.6 after five days. Therefore, the optimal data acquisition method fitting for a GEO SAR case is important to improve the GEO D-InSAR processing performance. Figure 1 is the instance to show the performance of the OMRD data acquisition method. The correlation coefficients due to the rotation-induced decorrelation in the two data acquisition methods are 0.523 (ZDC data acquisition method) and 0.996 (OMRD data acquisition method), respectively.

Moreover, as for the low frequency (e.g. L band) GEO SAR system, ionospheric disturbance has the obvious impacts on D-InSAR processing. The decorrelations of InSAR pair related to the image shifts and the interferometric phase screen errors brought by the temporal-spatial background ionosphere variation have been analyzed [30]. A simulation example based on United States Total Electron Content (USTEC) data released by the National Oceanic and Atmospheric Administration (NOAA) is given in Figure 2. The background ionosphere data in Isla Guadalupe Island (29.02°N, 118.27°W) at 7th and 8th October, 2013 is employed. The results suggest that the temporal-spatial background ionosphere variation can give rise to even the complete decorrelation in the InSAR pair and the produced interferometric phase screen error can correspond to a deformation measurement error of more than 0.2 m even in a not severely impacted area. Aimed at these problems, several methods could be utilized to eliminate such impacts. If the range and azimuth shifts are severe, a high accuracy co-registration should be adopted to solve the problem. Moreover, the interferometric phase screen error can be retrieved and compensated from the raw data, which uses low-resolution images and a set of stable points or regions to retrieve and correct the disturbed ionospheric phase screen [29]. Moreover, the azimuth shift can also be corrected in imaging based on coherent targets and the corresponding reference targets [13].

2.2 Limitation of GEO D-InSAR in deformation measurement

Although 1D deformation measurement of GEO D-InSAR has good deformation measurement accuracy, only a single direction (line-of-sight (LOS) direction) deformation cannot be accurate to fully evaluate the real surface deformations [5]. As shown in Figure 3, in the case of 1D deformation measurement,

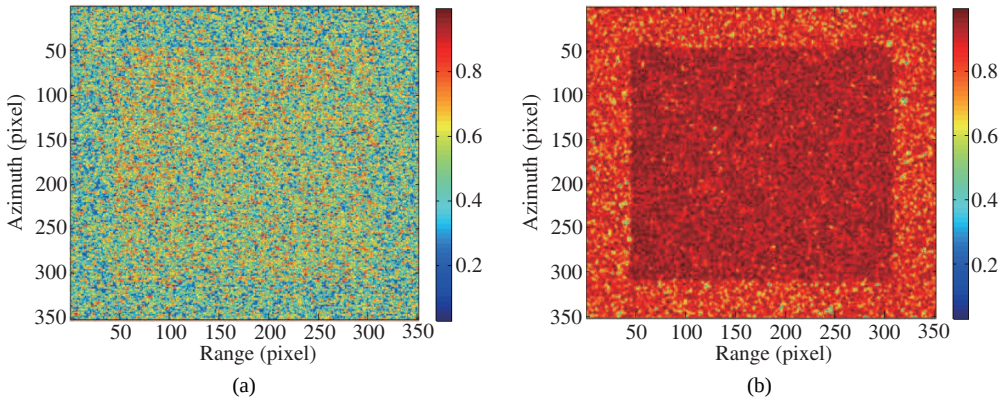

Figure 1 (Color online) Coherence maps of the GEO InSAR pairs corresponding to two data acquisition methods: (a) ZDC data acquisition method; (b) OMRD data acquisition method (Figure 6 in [23]).

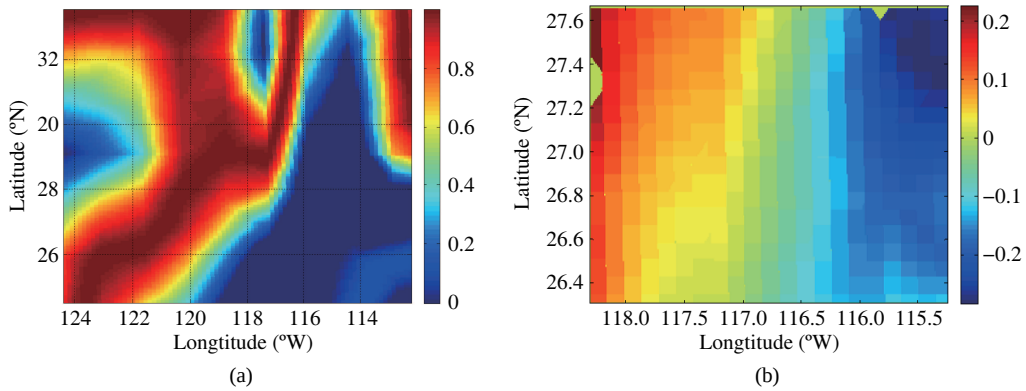

Figure 2 (Color online) Correlation coefficient only under the impacts of the azimuth relative shift (a) and the deformation retrieval error in a not severely impacted area (b) (Figure 5(d) and Figure 7(b) in [30]).

as the flight direction of the satellite is perpendicular to the north-south direction, the north-south direction deformation (the deformation marked as the green line) has a small projection component on the measurement direction. Resultantly, the LOS deformation measurement cannot measure the deformation in the north-south direction. Therefore, we need to carry out 3D deformation measurement through multi-angle data to obtain the complete deformation field information of the scene. Figure 3 is the schematic diagram of the 3D deformation measurement by SAR system. In the case of the observation at three angles, although the deformation has a small north-south direction projection component on the first observation angle, it has large north-south direction projection components on the second and the third observation angles and can be measured. Therefore, due to the angle difference of the multi-angle observation, it is possible to measure the 3D deformation field.

3 GEO SAR multi-angle measuring: 3D deformation retrieval

3.1 Theory and accuracy analysis

This section first explains the basic principle of GEO SAR 3D deformation retrieval by multi-angle measuring. The GEO SAR 3D deformation retrieval by multi-angle measuring is realized by selecting at least three angles (sub-apertures) for interferometry processing, which are utilized for obtaining the 3D deformation information of the scene. The basic sketch map of GEO SAR 3D deformation retrieval by multi-angle measuring is shown in Figure 4. $\boldsymbol{P}_0$ is the position of the target. $\boldsymbol{S}_1$, $\boldsymbol{S}_2$ and $\boldsymbol{S}_3$ represent three phase centers of the sub-apertures obtained in different angles. L_{a1}, L_{a2} and L_{a3} are the corresponding sub-apertures in the three angles. $\hat{\boldsymbol{E}}$ is the unit vector of the east-west direction, $\hat{\boldsymbol{N}}$ is the unit vector

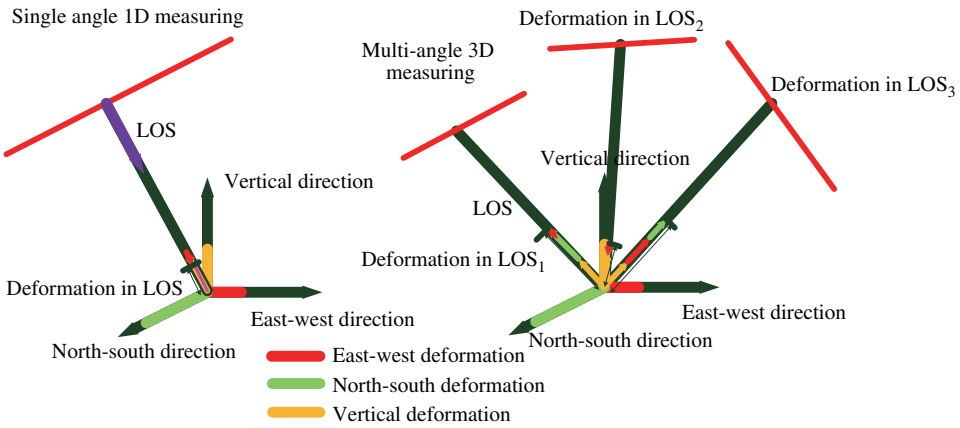

Figure 3 (Color online) Schematic diagram of the 1D and 3D deformation measurements by SAR system.

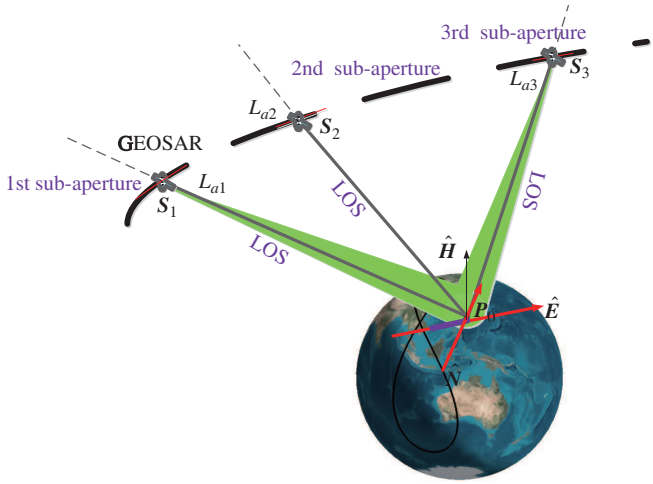

Figure 4 (Color online) Basic sketch map of GEO SAR 3D deformation retrieval by multi-angle measuring.

of the north-south direction, $\hat{\boldsymbol{H}}$ is the unit vector of the vertical direction. The black "figure 8" curve represents the nadir-point trajectory of a inclined geosynchronous orbit SAR satellite.

It can be seen from Figure 4 that the LOS deformation in each observation angle can be obtained. The estimation of the 3D deformation of the scene will be obtained through the least squared method of the interferometric phases of the three observation angles. Assuming the interferometric phases of angles L_{a1}, L_{a2} and L_{a3} are Φ_{s1}, Φ_{s2} and Φ_{s3}, the relationship between the multi-angle interferometric phases and the 3D deformation is expressed as

$$\boldsymbol{\Phi} = \boldsymbol{\Theta}\boldsymbol{d}, \tag{1}$$

where $\boldsymbol{\Phi} = (\Phi_{s1}, \Phi_{s2}, \Phi_{s3})^{\mathrm{T}}$ is the vector of the measured phases, $\boldsymbol{d} = (d_n, d_e, d_v)^{\mathrm{T}}$ is the 3D deformation vector in the local coordinate and the coefficient matrix $\boldsymbol{\Theta}$ is expressed as

$$\boldsymbol{\Theta} = \begin{bmatrix} \frac{\partial \Phi_{s1}}{\partial d_n} & \frac{\partial \Phi_{s1}}{\partial d_e} & \frac{\partial \Phi_{s1}}{\partial d_v} \\ \frac{\partial \Phi_{s2}}{\partial d_n} & \frac{\partial \Phi_{s2}}{\partial d_e} & \frac{\partial \Phi_{s2}}{\partial d_v} \\ \frac{\partial \Phi_{s3}}{\partial d_n} & \frac{\partial \Phi_{s3}}{\partial d_e} & \frac{\partial \Phi_{s3}}{\partial d_v} \end{bmatrix} = \begin{bmatrix} -\frac{4\pi}{\lambda}\left\langle \hat{\boldsymbol{R}}_{\boldsymbol{P}_0,\boldsymbol{S}_1}, \hat{\boldsymbol{N}} \right\rangle & -\frac{4\pi}{\lambda}\left\langle \hat{\boldsymbol{R}}_{\boldsymbol{P}_0,\boldsymbol{S}_1}, \hat{\boldsymbol{E}} \right\rangle & -\frac{4\pi}{\lambda}\left\langle \hat{\boldsymbol{R}}_{\boldsymbol{P}_0,\boldsymbol{S}_1}, \hat{\boldsymbol{H}} \right\rangle \\ -\frac{4\pi}{\lambda}\left\langle \hat{\boldsymbol{R}}_{\boldsymbol{P}_0,\boldsymbol{S}_2}, \hat{\boldsymbol{N}} \right\rangle & -\frac{4\pi}{\lambda}\left\langle \hat{\boldsymbol{R}}_{\boldsymbol{P}_0,\boldsymbol{S}_2}, \hat{\boldsymbol{E}} \right\rangle & -\frac{4\pi}{\lambda}\left\langle \hat{\boldsymbol{R}}_{\boldsymbol{P}_0,\boldsymbol{S}_2}, \hat{\boldsymbol{H}} \right\rangle \\ -\frac{4\pi}{\lambda}\left\langle \hat{\boldsymbol{R}}_{\boldsymbol{P}_0,\boldsymbol{S}_3}, \hat{\boldsymbol{N}} \right\rangle & -\frac{4\pi}{\lambda}\left\langle \hat{\boldsymbol{R}}_{\boldsymbol{P}_0,\boldsymbol{S}_3}, \hat{\boldsymbol{E}} \right\rangle & -\frac{4\pi}{\lambda}\left\langle \hat{\boldsymbol{R}}_{\boldsymbol{P}_0,\boldsymbol{S}_3}, \hat{\boldsymbol{H}} \right\rangle \end{bmatrix}. \tag{2}$$

According to (2), the phase sensitivity of the deformation measuring direction relates only to the coefficient matrix. The smaller the angle between the deformation measuring direction (LOS) and a component of the 3D deformation orthogonality basis is, the more sensitive the deformation measuring direction is to the component of the orthogonality basis. The phase sensitivity is independent of the deformation value.

Resolving (1), the estimation of $\boldsymbol{d}$ is given as

$$\hat{\boldsymbol{d}} = \left(\boldsymbol{\Theta}^{\mathrm{T}}\boldsymbol{C}_{\Phi}\boldsymbol{\Theta}\right)^{-1}\boldsymbol{\Theta}^{\mathrm{T}}\boldsymbol{C}_{\Phi}\boldsymbol{\Phi}, \tag{3}$$

where $\boldsymbol{C}_{\Phi}$ is the covariance matrix of the measured phase. Assuming the three observation angles are independent, the interferograms of different observation angles and the deformations in different directions are not correlated. Therefore, the non-diagonal elements in $\boldsymbol{C}_{\Phi}$ are zero. $\boldsymbol{C}_{\Phi}$ is only determined by its diagonal elements, which are shown as

$$\boldsymbol{E}_{\Phi} = \mathrm{diag}(\boldsymbol{C}_{\Phi}) = \left(\sigma^2_{\Phi_{s1}}, \sigma^2_{\Phi_{s2}}, \sigma^2_{\Phi_{s3}}\right)^{\mathrm{T}}, \tag{4}$$

where $\boldsymbol{E}_{\Phi}$ is the variance vector of the phase, $\mathrm{diag}(\cdot)$ is the operation for extracting the diagonal elements of the matrix.

According to (3), the estimated covariance matrix of the deformation $\boldsymbol{C}_{\hat{d}}$ is expressed as

$$\boldsymbol{C}_{\hat{d}} = \left(\boldsymbol{\Theta}^{\mathrm{T}}\boldsymbol{C}_{\Phi}\boldsymbol{\Theta}\right)^{-1}. \tag{5}$$

Then, the variance vector of the deformation can be expressed as

$$\boldsymbol{E}_{\hat{d}} = \mathrm{diag}(\boldsymbol{C}_{\hat{d}}) = \left(\sigma^2_{d_n}, \sigma^2_{d_e}, \sigma^2_{d_v}\right)^{\mathrm{T}}. \tag{6}$$

From (6), the smaller the phase noise of the interferogram is, the higher the obtained 3D deformation retrieval accuracy is . In the meantime, $\boldsymbol{C}_{\hat{d}}$ relates to $\boldsymbol{\Theta}$. Thus, 3D deformation retrieval accuracy also depends on the orbital configuration and the geo-location of the observed area, which will be discussed in the next section.

3.2 Optimal multi-angle data selection

In general, the accuracy of the GEO SAR multi-angle 3D deformation retrieval depends on the coefficient matrix (i.e. spatial position of the satellite and the scene). Observation scenarios are generally determined by the actual application requirements, which cannot be arbitrarily changed. Therefore, to obtain the best 3D deformation retrieval performance, it is necessary to study the optimal multi-angle data acquisition (the positions of sub-apertures) within the GEO SAR trajectory part for observing the scene. However, in practice, due to the complex geometric configuration of GEO SAR orbits, it is impossible to find the appropriate multi-angle (three observation angles) for data acquisition to minimize the deformation measurement errors in three dimensions simultaneously. Therefore, the holistical 3D deformation retrieval accuracy should be considered to select the optimal multi-angle data.

Here, we introduce the concept of geometric dilution of precision (GDOP) in global navigation satellite system (GNSS) to evaluate the accuracy of the multi-angle data for the 3D deformation retrieval [31]. Since there is no clock timing bias in SAR, GDOP will be determined by the position dilution of precision (PDOP) in our analysis. The PDOP is mainly characterized by the spatial configuration of the multi-angle geometry for the 3D deformation retrieval. A poorer spatial configuration will result in a higher PDOP value.

According to the definition of PDOP, assuming the phase variance of interferograms in different angles are same (σ_e^2), we define the 3D deformation measurement accuracy coefficient as

$$\mathrm{PDOP}_m = \sqrt{\frac{16\pi^2\Lambda}{\lambda^2\sigma_e^2}}, \tag{7}$$

where

$$\Lambda = \sqrt{\boldsymbol{E}_{\hat{d}}^{\mathrm{T}}\boldsymbol{E}_{\hat{d}}} \tag{8}$$

is the square root of the sum of the variances in three dimensions, representing the holistic 3D deformation measurement accuracy.

Considering (8), Eq. (7) can be simplified as

$$\mathrm{PDOP}_m = \sqrt{\frac{16\pi^2}{\lambda^2}\mathrm{tr}\left[\left(\boldsymbol{\Theta}^{\mathrm{T}}\boldsymbol{\Theta}\right)^{-1}\right]}, \tag{9}$$

where $\mathrm{tr}\,(\cdot)$ represents the trace of a matrix.

By (9), it is more intuitive to find that PDOP_m is directly associated with the coefficient matrix. As a small PDOP_m will be helpful for improving the 3D deformation retrieval accuracy, to find the optimal multi-angle data to obtain the best holistic 3D deformation measurement accuracy, we need to consider

$$\min_{\boldsymbol{S}_1,\boldsymbol{S}_2,\boldsymbol{S}_3}\left\{\mathrm{PDOP}_m\left(\boldsymbol{P},\boldsymbol{S}_1,\boldsymbol{S}_2,\boldsymbol{S}_3\right)\right\} \quad \text{s.t.} \quad \{\boldsymbol{S}_1,\boldsymbol{S}_2,\boldsymbol{S}_3\} \in \boldsymbol{S}_a, \tag{10}$$

where $\boldsymbol{P}$ is the position vector of the center of the scene, $\boldsymbol{S}_a$ represents the GEO SAR trajectory part which can observe the scene.

The analytical solution of (10) is difficult to be directly obtained due to the complex trajectory of GEO SAR. At the same time, because of the long observation time and large observation area of GEO SAR system, it is not of high efficiency to obtain the optimal multi-angle data and 3D deformation accuracy of each ground observation position by the searching algorithm along $\boldsymbol{S}_a$. To solve this problem, the searching algorithm can be firstly used to obtain the solutions of (10) for a number of ground observation sample points. Then, the neural networks can be constructed to obtain the results of the whole observation region of interest. Neural networks are very good at solving the problem with a complex mathematical model [32]. After learning many times, the adaptability of model parameters is realized. The data calculation accuracy and the convergence rate can suit for the practical applications [33]. Therefore, based on the basic principles of neural networks, our model is set as

$$\boldsymbol{y}_i = f_i(\boldsymbol{w}_i^{\mathrm{T}}\boldsymbol{x}_i - \theta_{i,j}), \tag{11}$$

where i represents the ith layer of the neural network, $\boldsymbol{x}_i$ is the input of the neuron in the ith layer, $\boldsymbol{y}_i$ is the output of the neuron in the ith layer, $\boldsymbol{w}_i$ is the weight of the neuron in the ith layer, $\theta_{i,j}$ is the threshold of the jth neuron in the ith layer, f_i is the activation function of the neuron in the ith layer, which is usually the nonlinear sigmoid function, shown as

$$f(x) = \frac{1}{1+\mathrm{e}^{-x}}. \tag{12}$$

When we conduct the training for samples, the input samples have two characteristics: longitude lon and latitude lat of the objective graphical region for analysis. The outputs are the minimal PDOP_{m_o} and the corresponding true anomalies of the multi-angle positions A_{S_1}, A_{S_2} and A_{S_3}, which represent the solution for the optimal multi-angle data selection for 3D deformation retrieval. In fact, they are accordance with the parameters in (10) and derive from it. Thus, the input vector $\boldsymbol{x}_1$ and the output vector $\boldsymbol{y}_e$ can be expressed as

$$\begin{cases} \boldsymbol{x}_1 = (\mathrm{lat}, \mathrm{lon})^{\mathrm{T}}, \\ \boldsymbol{y}_e = \left(\mathrm{PDOP}_{m_o}, A_{S_1}, A_{S_2}, A_{S_3}\right)^{\mathrm{T}}. \end{cases} \tag{13}$$

Based on the above analysis, the complete 3D deformation retrieval based on GEO SAR multi-angle processing is depicted in Figure 5, which is summarized as:

Step 1: Based on the region of interest, GEO SAR orbit and the steering capability of the GEO SAR system (the look angle variation scope and the ground squint angle scope), calculating the required look angle and the long coverage GEO SAR orbit part which can observe the target region;

Step 2: Using searching algorithm with the objective function of (10) to determine the optimal sub-aperture locations for multi-angle data acquisition, which can minimize the PODP value by the selected sub-apertures;

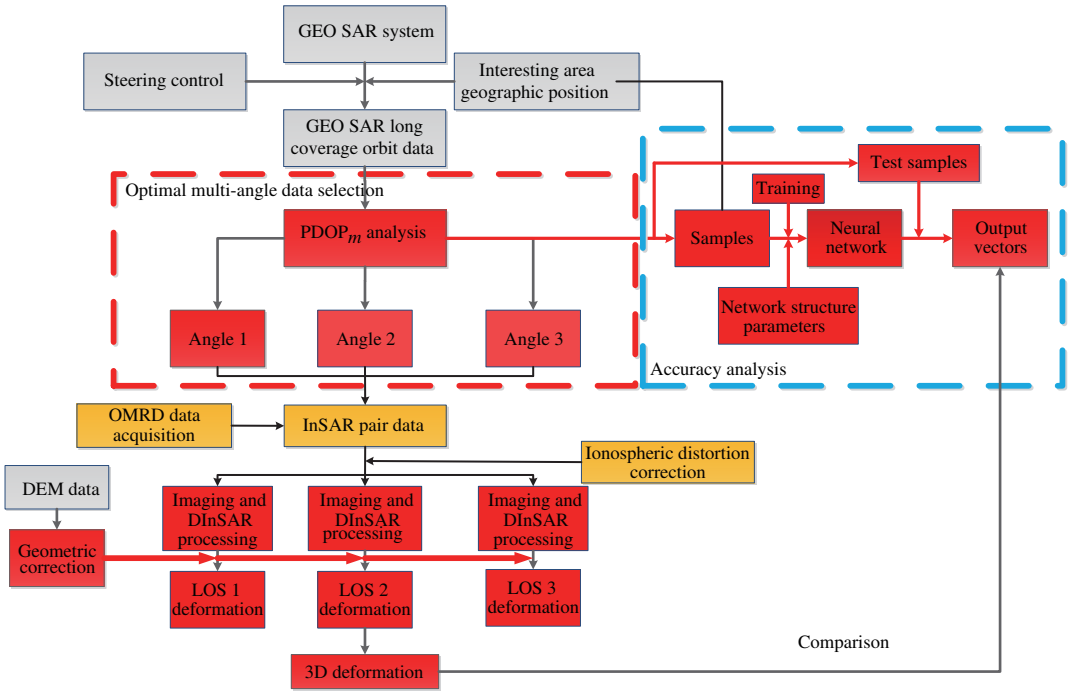

Figure 5 (Color online) Flow chart of the 3D deformation retrieval based on GEO SAR multi-angle processing.

Table 1 GEO SAR orbit and system parameters

Item	Value	Item	Value
Semi-major axis (km)	42164.170	True anomaly (°)	0
Inclination (°)	53	Eccentricity	0.07
Argument of perigee (°)	270	Right ascension of ascending node (°)	265
Wavelength (m)	0.24	Bandwidth (MHz)	18

Step 3: Realizing the optimal InSAR pair data acquisition based on the method in [23] and completing imaging and interferometry processing; compensating the ionospheric disturbance phase by using the ionospheric phase screen model in [30];

Step 4: Co-registering the interferograms obtained at different angles by using external DEM data;

Step 5: Generating the LOS deformations at different angles and realizing 3D deformation retrieval of the scene according to (3);

Step 6: Utilizing PDOP analysis to calculate the 3D deformation retrieval accuracy of the samples in the scene, and obtaining the 3D deformation retrieval accuracy of the whole scene by neural network, which will be compared with the simulated 3D deformation retrieval results.

4 Simulation and discussion

In the simulation, we use the GEO SAR orbit with a large "figure 8" nadir-point trajectory. The orbit position at apogee is selected as an instance for the following processing. The geographic position of the center of the scene is (40°N, 105°E). The orbit and system parameters of GEO SAR are given in Table 1.

4.1 Simulation validation of the optimal multi-angle data selection

According to the analysis in Subsection 3.2, the selection of the multi-angle data directly affects the accuracy of GEO SAR 3D deformation retrieval. Therefore, we first simulate and discuss the optimal multi-angle data selection for GEO SAR 3D deformation retrieval. The antenna has the ability to be continuously steered, and only has the right-look ability. The look angle ranges from 1° to 8° and the

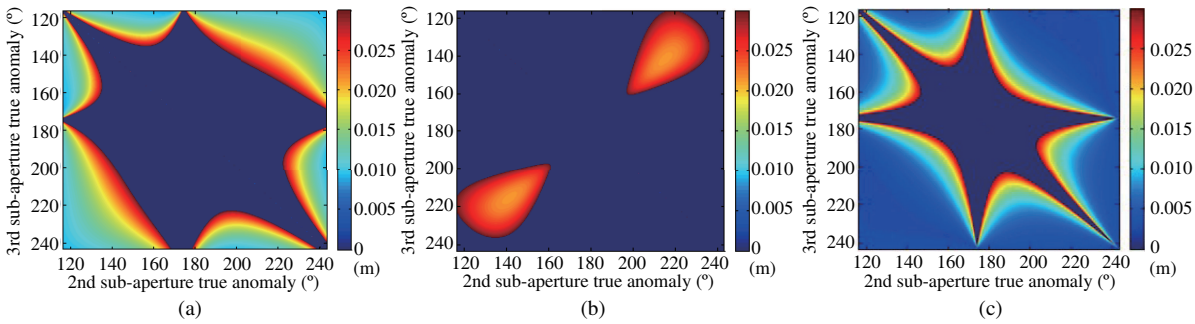

Figure 6 (Color online) 3D deformation retrieval accuracies of different positions of the two angles (the area with the accuracy worse than 0.03 m has been excluded (the darkest part of the figures)). (a) North-south direction; (b) east-west direction; (c) vertical direction.

ground squint angle of GEO SAR is limited within ±60°. In this case, the GEO SAR can keep observing the scene within a true anomaly scope of [116.4°, 243.4°]. When all the positions of the three angles used for 3D deformation retrieval are changed along the GEO SAR orbit, the whole optimization space is a spatial topology, which is very complicated. In order to simplify the calculation, in the following simulation analysis, we assume that the position of the first aperture is known. It is at a position in the full aperture (true anomaly is 174.4°) obtained at the ground 0° squint angle and 2° look angle. Then, the 3D deformation retrieval performance is investigated by selecting the other two angles (sub-apertures) along the orbit scope with the capability of observing the scene. Figure 6 is the obtained 3D deformation retrieval accuracies when the positions of the two angles change.

From Figure 6, it can be observed that a large error in the 3D deformation retrieval will be introduced when two or more angles have the same or similar positions (corresponding to the darkest-colored region in Figure 6). When the positions of at least two angles are accordance, theoretically, 3D deformation retrieval is impossible. The bias between the positions of the angles will be helpful to improve the 3D deformation retrieval accuracy. In addition, according to Figure 6, the deformation accuracies in different directions are largely difference. The deformation measurement accuracy in vertical direction is higher than those of the other two directions by an order of magnitude. The deformation measurement accuracy in the east-west direction is larger by a factor 2 than that in the north-south direction. This phenomenon is mainly due to the different sensitivities of the deformation measurements in three directions. The deformation measurement sensitivity analysis in different directions is shown in Figure 7. The deformation measurement sensitivity in the vertical direction is the highest among the three directions.

As the optimal positions of the deformation measurement accuracy in different directions are different, we should determine the optimal multi-angle positions for GEO SAR 3D deformation measurement based on the method of PDOP analysis. The PDOP analysis of the selection of other two multi-angle positions is shown in Figure 8. As shown in Figure 8, when the true anomalies of the three angles are (132.1°, 174.4°, 222.4°) (marked as cross star), the holistic 3D deformation retrieval accuracy is the optimal, which has only a PDOP of 6.2 . Under such multi-angle data selection, the 3D deformation measurement accuracies are 0.009 m (north-south direction), 0.021 m (east-west direction) and 0.003 m (vertical direction). Since the east-west direction has the worst deformation measurement accuracy, its accuracy has the greatest effect on the PDOP. Comparing Figure 6(b) and Figure 8, it can be found that the location of the multi-angle positions determined optimally by PDOP is closer to the position with the best deformation measurement accuracy in the east-west direction. Finally, the multi-angle data selected by optimal PDOP makes the deformation measurement accuracy in the three dimensions all less than 2.1 cm.

According to the optimal multi-angle positions, we study the relationship of the angles between the link lines of the three phase centers of the sub-apertures, which is shown in Figure 9(a). The angles between the three link lines are 62°, 40°, and 78°, respectively (clockwise). Compared with the angles between the three link lines of the phase centers of the optimal three sub-apertures in GEO CSAR (Figure 9(b)), which are all 60° [25], there is an obvious difference. The difference derives from the following two aspects:

1) The inclined "figure 8" GEO SAR orbit is affected by the earth rotation and orbit perturbation,

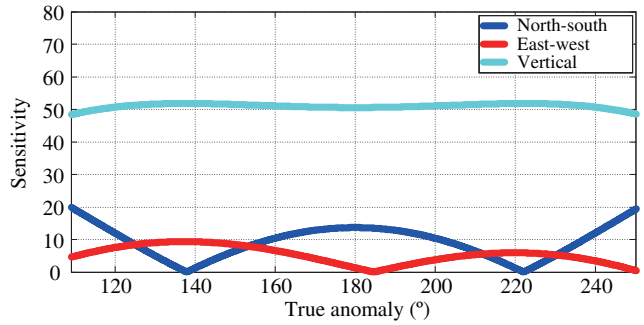

Figure 7 (Color online) Deformation measurement sensitivity analysis in different directions.

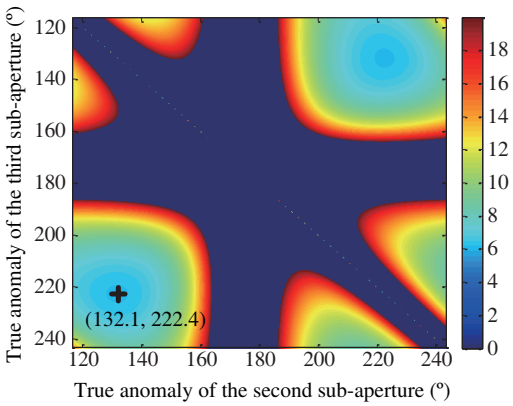

Figure 8 (Color online) PDOP analysis of the selection of other two multi-angle positions (assuming the correlation coefficient of a single interferogram is 0.95).

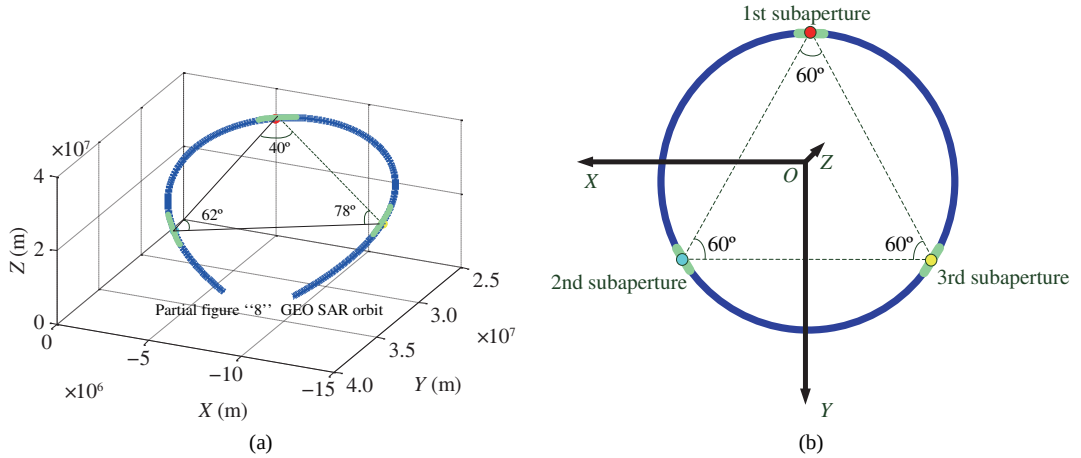

Figure 9 (Color online) Relationship of the angles between the link lines of the three phase centers of the multi-angle data. (a) Inclined GEO SAR; (b) GEO CSAR.

which make trajectory very curved (like a 'collar' edge). It is not a standard circle, which is pear-like or elliptical;

2) The steering capability of the actual GEO SAR satellite system is limited and the system cannot stare at the target all the time. Thus, only part of the orbit (part of the spatial angle scope) can be used for multi-angle data acquisition.

Therefore, as the influence of the aforementioned factors, the spatial configuration of the optimal multi-angle data in a inclined orbit GEO SAR case is different from that in GEO CSAR.

4.2 3D deformation retrieval simulation

In this sub-section, we will exhibit the results of the 3D deformation retrieval. The scene of interest is 7 km × 7 km. There is a 260 m high pyramid in the scene. We generate the deformation in the pyramid area. The vertical deformation is 2 cm, decreasing linearly from the peak to the bottom. There are about 0.26 m deformation and no deformation in the east-west direction and north-south direction, respectively. The integration time is 100s. The temporal baseline is 1 day. In the following processing, we only consider the single look processing and the Goldstein phase filtering coefficient is 0.1. The positions of the multi-angle data used in the following simulation are shown in Figure 10. A to E represent the five positions of the utilized multi-angle data and the corresponding true anomalies are also marked in the Figure 10. The covered yellow line along the nadir-point trajectory represents the orbit scope which can observe the target.

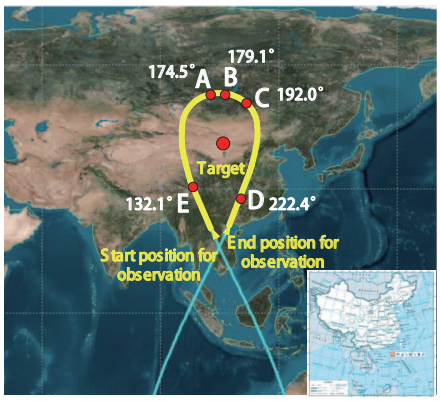

Figure 10 (Color online) Positions of the multi-angle data used in the simulation.

Two simulation groups are conducted and their results are compared. We first use the multi-angle data with the sub-apertures of A, B and C (true anomalies are 174.4°, 179.1° and 192.0°) for the 3D deformation retrieval, which has a theoretical PDOP value of 106 (assuming the correlation coefficient of a single interferogram is 0.95). In the comparison group, the optimal multi-angle data, including the sub-apertures of A, D, and E (true anomalies are 132.1°, 174.4° and 222.4°), is selected (theoretical PDOP = 6.2 for this group). The interferograms of the sub-apertures all have the high coherence coefficients above 0.8 (0.91 (A), 0.91 (B), 0.83 (C), 0.91 (D), and 0.89 (E)). The original set 3D deformation and the 3D deformation retrieval results are shown in Figure 11. The corresponding error analysis is provided in Table 2. Because of the non-optimal sub-apertures, the deformation measurement accuracy in the north-south is worse in the first group, which is more than 20 cm. In addition, its east-west deformation measurement accuracy (ten-centimeter level) and vertical deformation measurement accuracy (centimeter-level) are not very high as well. In comparison, when the optimal sub-apertures are selected, all the deformation measurement accuracies in the three dimensions are improved significantly. Both the east-west and north-south deformation measurement accuracies are centimeter-level, and the vertical deformation measurement even reaches to millimeter-level. Therefore, the simulation results suggest the importance of the optimal sub-aperture selection.

4.3 Analysing the impacts of orbit configuration and geographical position of scene on 3D deformation retrieval accuracy

Three classical GEO SAR orbits are used in the sub-section for studying the impacts of orbit and geographical position of scene on 3D deformation retrieval accuracy. Although they are all geosynchronous orbits, they have different orbit elements (e.g. eccentricity and inclination). The prime orbit elements of the three classical GEO SAR orbits are listed in Table 3 and the nadir-point trajectories are given in Figure 12(a). Large "figure 8" and "figure O" are set to work in right-look for obtaining good coverage performance for China. In contrast, small "figure 8" is designed to work in left-look to obtain good coverage performance for China.

In the simulation, we use the neural network method described in Section 3 for the analysis. We selected 44 samples (43 in China and 1 in Singapore) in the following simulation, which are shown in Figure 12(b). The training set constitutes 39 training samples and the test set has 5 samples. We have constructed a three-layer Back Propagation (BP) neural network. Each layer of the neural network includes 10 neurons. Sigmoid function is selected as the activation function. To reduce computation burden, we assume that the position of the first angle is known, which locates at the start of the orbit scope for observing the target. Then, the optimal positions of the other two angles are analyzed, which means the output vector $\boldsymbol{y}_e = (\mathrm{PDOP}_{m_o}, A_{S_2}, A_{S_3})^{\mathrm{T}}$. The holistic 3D deformation retrieval accuracies Λ under the three orbits and the different geographical positions within China and the coverage maps for China are given in Figure 13.

Comparing the results of Figures 13 (a), (b) and (c), it can be seen that among the three orbits

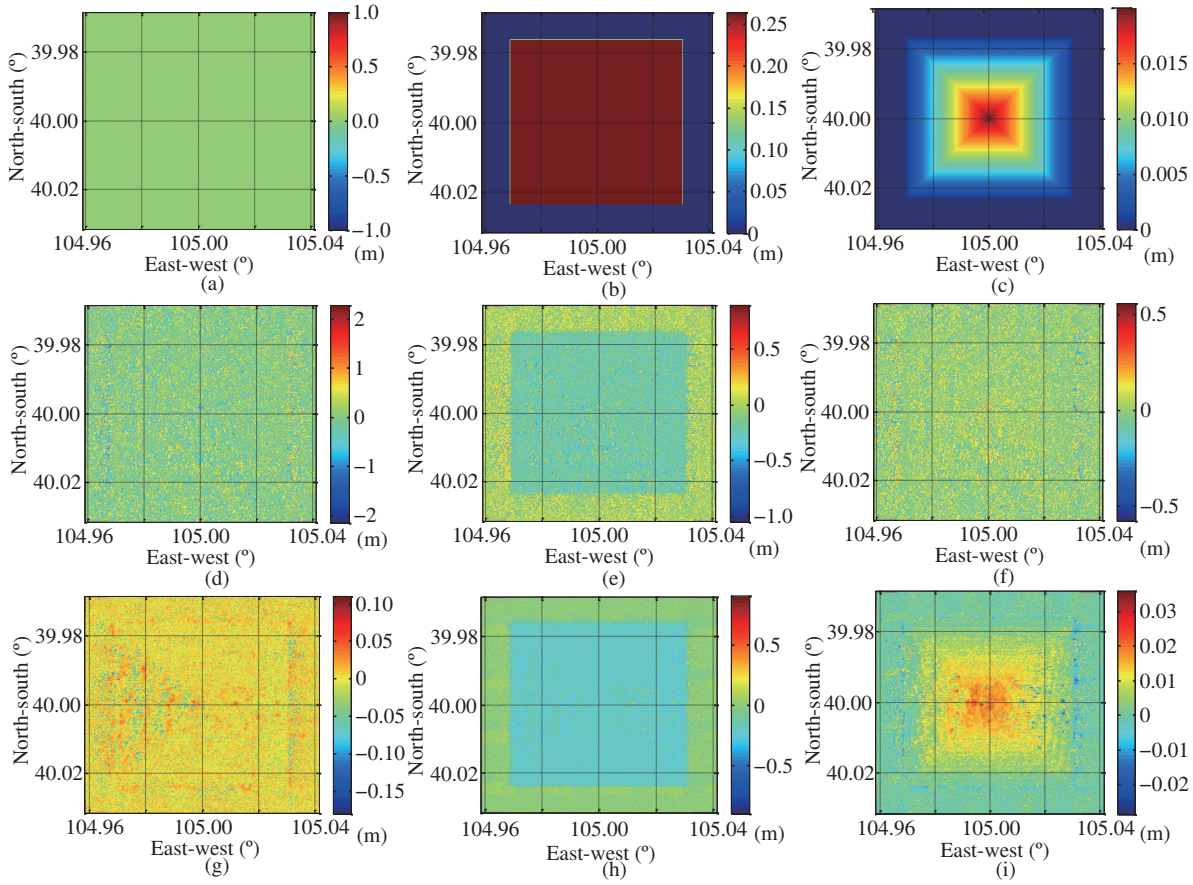

Figure 11 (Color online) Results of the 3D deformation retrieval. Original deformation: (a) north-south direction (N-S); (b) east-west direction (E-W); (c) vertical direction (VD). The first group (A+B+C): (d) N-S; (e) E-W; (f) VD. The second group (A+D+E): (g) N-S; (h) E-W; (i) VD.

Table 2 3D deformation retrieval accuracy evaluation (RMSE analysis)

Group No.	North-south direction (cm)	East-west direction (cm)	Vertical direction (cm)
1	28.6	11.5	7.5
2	1.72	6.27	0.35

Table 3 Prime orbit elements of the three classical GEO SAR orbits

Nadir-point trajectory	Large "figure 8"	Small "figure 8"	"figure O"
Eccentricity	0.07	0.05	0.1
Inclination (°)	53	0	16

shown in Table 3, the large "figure 8" orbit has the best holistic 3D deformation retrieval accuracy, which reaches to centimeter-lever in the most part of China. The holistic 3D deformation retrieval accuracy even reaches to millimeter-level in the Qinghai-Tibet Plateau of China; Small "figure 8" has the worst holistic 3D deformation retrieval accuracy, which is close to meter-level. The 3D deformation retrieval accuracy in the east part of China is about 10 cm, which is better than that in the west area of China; "figure O" has a moderate 3D deformation retrieval accuracy, which ranges from several centimeters to dozens of centimeters. 3D deformation retrieval accuracy in the south is better than that in the north in the "figure O" case. Various 3D deformation retrieval accuracies derive from different orbit configurations. According to Figure 12(a), the observation angle scope of the large "figure 8" is the greatest for observing China among the three orbits, which results in a small correlation of each row in the observation matrix. Thus, its 3D deformation retrieval accuracy is the best. In contrast, as the observation angle scope of

Figure 12 (Color online) Nadir-point trajectories of the three GEO SAR orbits (a) and the distribution of the samples (b).

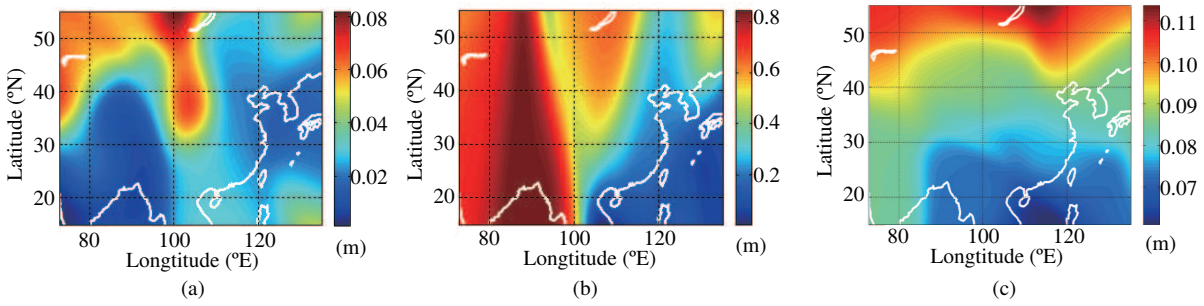

Figure 13 (Color online) Holistic 3D deformation retrieval accuracies under the three orbits and the different geographical positions (a) large "figure 8"; (b) small "figure 8"; (c) "figure O".

the large small "figure 8" is very small, its 3D deformation retrieval accuracy is poor.

5 Conclusion

This paper focuses on the method and performance analysis of 3D deformation retrieval based on GEO SAR multi-angle processing. To obtain the optimal accuracy, an optimal selection method of GEO SAR multi-angle data by minimizing PDOP is proposed. Moreover, to improve the computation efficiency, neural network is utilized for analyzing the 3D deformation retrieval accuracy under the different orbit configurations and target geo-locations. Finally, simulation experiments are conducted to verify the theoretical analysis. Several important conclusions are as follows:

(1) With respect to 3D deformation retrieval, two or more angles should be avoided to have the same or similar positions for improving the 3D deformation retrieval accuracy. As the deformation measurement sensitivities in three directions are different, the deformation retrieval accuracies in three directions also have a large bias. Take the "figure 8" orbit as an example, the deformation measurement accuracy in vertical direction is higher than those of the other two directions.

(2) The optimal positions of the deformation measurement accuracy in different directions are different. As a result, to determine the optimal multi-angle data for GEO SAR 3D deformation measurement based on the method of the optimal PDOP analysis is needed. The location of the optimal multi-angle positions determined optimally by PDOP mainly depends on the deformation measurement direction with the worst accuracy.

(3) The optimal multi-angle positions in the inclined GEO SAR orbit case has differences with that

in a standard CSAR orbit case. The angles between the link lines of the three phase centers of the multi-angle data in the inclined GEO SAR case are not all 60° due to the complex orbit shape and the limited steering capability of the system.

(4) Orbit configurations and locations of scene have a large impacts on the GEO SAR 3D deformation retrieval accuracy. In the best case of the analyzed orbits, large "figure 8", it has the best holistic 3D deformation retrieval accuracy, which reaches to centimeter-lever.

Acknowledgements This work was supported by National Natural Science Foundation of China (Grant Nos. 61427802, 61471038, 61501032), Chang Jiang Scholars Program (Grant No. T2012122), 111 Project of China (Grant No. B14010), and China Scholarship Council (CSC).

Conflict of interest The authors declare that they have no conflict of interest.

References

1 Massonnet D, Rossi M, Carmona C, et al. The displacement field of the Landers earthquake mapped by radar interferometry. Nature, 1993, 364: 138–142
2 Ferretti A, Monti Guarnieri A, Prati C, et al. InSAR Principles. Netherlands: ESA Publications, 2007. B-11-CB-55
3 Huang R Q, Fan X M. The landslide story. Nature Geosci, 2013, 6: 325–326
4 Hu J, Li Z W, Ding X L, et al. 3D coseismic Displacement of 2010 Darfield, New Zealand earthquake estimated from multi-aperture InSAR and D-InSAR measurements. J Geodesy, 2012, 86: 1029–1041
5 Wright T J, Parsons B E, Zhong L. Toward mapping surface deformation in three dimensions using InSAR. Geophys Res Lett, 2004, 31: L01607
6 Ansari H, De Zan F, Parizzi A, et al. Measuring 3D surface motion with future SAR systems based on reflector antennae. IEEE Geosci Remote Sens Lett, 2016, 13: 272–276
7 Gudmundsson S, Sigmundsson F, Carstensen J M. Three-dimensional surface motion maps estimated from combined interferometric synthetic aperture radar and GPS data. J Geophys Res, 2002, 107: ETG 13-1C-ETG 13-14
8 Tomiyasu K. Synthetic aperture radar in geosynchronous orbit. In: Proceedings of IEEE Antennas and Propagation Society International Symposium, College Park, 1978. 42–45
9 Prati C, Rocca F, Giancola D, et al. Passive geosynchronous SAR system reusing backscattered digital audio broadcasting signals. IEEE Trans Geosci Remote Sens, 1998, 36: 1973–1976
10 Bruno D, Hobbs S E, Ottavianelli G. Geosynchronous synthetic aperture radar: Concept design, properties and possible applications. Acta Astronaut, 2006, 59: 149–156
11 Monti Guarnieri A, Bombaci O, Catalano T F, et al. ARGOS: a fractioned geosynchronous SAR. Acta Astronaut, in press
12 Monti Guarnieri A, Broquetas A, Recchia A, et al. Advanced radar geosynchronous observation system: ARGOS. IEEE Geosci Remote Sens Lett, 2015, 12: 1406–1410
13 Hobbs S, Mitchell C, Forte B, et al. System design for geosynchronous synthetic aperture radar missions. IEEE Trans Geosci Remote Sens, 2014, 52: 7750–7763
14 Hu C, Long T, Zeng T, et al. The accurate focusing and resolution analysis method in geosynchronous SAR. IEEE Trans Geosci Remote Sens, 2011, 49: 3548–3563
15 Bruno D, Hobbs S E. Radar imaging from geosynchronous orbit: temporal decorrelation aspects. IEEE Trans Geosci Remote Sens, 2010, 48: 2924–2929
16 Ding Z G, Yin W, Zeng T, et al. Radar parameter design for geosynchronous SAR in squint mode and elliptical orbit. IEEE J Sel Top Appl Earth Observ Remote Sens, 2016, 9: 2720–2732
17 Dong X C, Hu C, Tian W M, et al. Feasibility study of inclined geosynchronous SAR focusing using Beidou IGSO signals. SCI China Inf Sci, 2016, 59: 129302
18 Recchia A, Monti Guarnieri A, Broquetas A, et al. Impact of scene decorrelation on geosynchronous SAR data focusing. IEEE Trans Geosci Remote Sens, 2016, 54: 1635–1646
19 Ding Z G, Shu B Z, Yin W, et al. A modified frequency domain algorithm based on optimal azimuth quadratic factor compensation for geosynchronous SAR imaging. IEEE J Sel Top Appl Earth Observ Remote Sens, 2015, 9: 1119–1131
20 Ruiz Rodon J, Broquetas A, Monti Guarnieri A, et al. Geosynchronous SAR focusing with atmospheric phase screen retrieval and compensation. IEEE Trans Geosci Remote Sens, 2013, 51: 4397–4404
21 Li Y H, Hu C, Dong X C, et al. Impacts of ionospheric scintillation on geosynchronous SAR focusing: preliminary experiments and analysis. Sci China Inf Sci, 2015, 58: 109301
22 Hu C, Li Y H, Dong X C, et al. Performance analysis of L-band geosynchronous SAR imaging in the presence of ionospheric scintillation. IEEE Trans Geosci Remote Sens, 2017, 55: 159–172
23 Hu C, Li Y H, Dong X C, et al. Optimal data acquisition and height retrieval in repeat-track geosynchronous SAR interferometry. Remote sens, 2015, 7: 13367–13389
24 NASA, JPL. Global Earthquake Satellite System, a 20 year plan to enable earthquake prediction. 2003
25 Kou L L, Wang X Q, Xiang M S, et al. Interferometric estimation of three-dimensional surface deformation using geosynchronous circular SAR. IEEE Trans Aerosp Electron Syst, 2012, 48: 1619–1635

26 Hobbs S. GeoSAR: Summary of the Group Design Project MSc in Astronautics and Space Engineering 2005/06 Cranfield University. College of Aeronautics Report 0509. Cranfield University. 2006
27 Hu C, Li X R, Long T, et al. GEO SAR interferometry: theory and feasibility study. In: Proceedings of IET International Radar conference, Xi'an, 2013. 1–5
28 Monti Guarnieri A, Tebaldini S, Rocca F, et al. GEMINI: geosynchronous SAR for Earth monitoring by interferometry and imaging. In: Proceedings of IEEE International Geoscience and Remote Sensing Symposium, Munich, 2012. 210–213
29 Ruiz-Rodon J, Broquetas A, Makhoul E, et al. Nearly zero inclination geosynchronous SAR mission analysis with long integration time for Earth observation. IEEE Trans Geosci Remote Sens, 2014, 52: 6379–6391
30 Hu C, Li Y H, Dong X C, et al. Impacts of temporal-spatial variant background ionosphere on repeat-track GEO D-InSAR system. Remote sens, 2016, 8: 916
31 Dana P H. Global positioning system overview. Department of Geography, University of Texas at Austin. 2000. http://www.colorado.edu/geography/gcraft/notes/gps/gps_f.html
32 Stramondo S, Del Frate F, Picchiani M, et al. Seismic source quantitative parameters retrieval from InSAR data and neural networks. IEEE Trans Geosci Remote Sens, 2011, 49: 96–104
33 Lippmann R. An introduction to computing with neural nets. IEEE Assp Mag, 1987, 4: 4–22